



Characteristics of Raindrop Size Distribution in Seoul, South Korea According to Rain and Weather Types

Minchae Jwa¹ · Han-Gyul Jin¹ · Joohyun Lee¹ · Sungju Moon¹ · Jong-Jin Baik¹

Received: 18 March 2020 / Revised: 15 July 2020 / Accepted: 24 August 2020 / Published online: 28 August 2020
© Korean Meteorological Society and Springer Nature B.V. 2020

Abstract

The raindrop size distribution (RSD) is useful in understanding various precipitation-related processes. Here, we analyze disdrometer data collected in Seoul, South Korea from May 2018 to July 2019 to characterize the RSD according to rain and weather types. Rain types are categorized into stratiform, mixed, and convective rain, and weather types into the Changma front (type CF) and low-pressure system (type L). The slope parameter Λ decreases and the intercept parameter N_0 fluctuates with rain rate. Among the rain types, the RSD of stratiform (convective) rain shows the steepest (mildest) slope and the smallest (largest) mean diameter. The logarithm of generalized intercept parameter $\log_{10}N_w$ and Λ for stratiform rain have considerably dispersed distributions, which may be attributed to the diversity within the stratiform rain type in Seoul. Mixed-type rain has a larger mean value of $\log_{10}N_w$ compared to stratiform and convective rain. Regarding the weather types, the RSD of type CF exhibits a milder slope, a larger mass-weighted mean diameter, and a larger radar reflectivity than type L. These differences between the weather types can be explained by the larger convective proportion in type CF (33%) compared to type L (9%). Possible causes for the differences between the RSD characteristics of the two weather types are examined using reanalysis and satellite data. Type CF has a larger convective available potential energy, a higher cloud top, and more active ice microphysical processes than type L, which can lead to different RSD characteristics.

Keywords Raindrop size distribution · Disdrometer · Rain type · Weather type · Seoul

1 Introduction

The raindrop size distribution (RSD) provides important pieces of information about clouds and precipitation and is one of the properties that can be observed directly using instruments such as disdrometers. Characterizing the RSD for different environmental conditions constitutes an important part of cloud and precipitation research (Pruppacher and Klett 2010), and a detailed analysis of direct observation data can play a part in advancing our understanding of clouds and precipitation.

The RSD characteristics are different depending on the rain type, namely stratiform and convective rain. Each type of rain is known to originate from different precipitating clouds and

may occur separately or together in a cloud complex (Houze 2014). Using ground-based disdrometers, many studies have shown that stratiform rain has high number concentration of small raindrops and a steep slope of the RSD, whereas convective rain has high number concentration of large raindrops and a mild slope of the RSD (e.g., Niu et al. 2010; Chen et al. 2017; Seela et al. 2018). Knowing the characteristics of the RSD for each of these rain types is helpful in understanding various cloud-related processes (Sui et al. 2007). For this reason, RSD characteristics of various regions have been analyzed according to the rain type (You et al. 2005; Chen et al. 2013; Suh et al. 2016; Das et al. 2017; Seela et al. 2018; Sreekanth et al. 2019; Wen et al. 2019; Wu et al. 2019). In addition, You et al. (2005) and Chen et al. (2013) obtained the Z – R (radar reflectivity–rain rate) relationship for each rain type and argued the possibility of improving the existing radar rainfall estimation using a single Z – R relationship.

The characteristics of RSD also vary depending on the weather type. Different weather types exhibit different compositions of stratiform and convective rain. Zhang et al. (2017) showed that the RSD characteristics of a midlatitude

Responsible Editor: Jinwon Kim.

✉ Jong-Jin Baik
jjbaik@snu.ac.kr

¹ School of Earth and Environmental Sciences, Seoul National University, Seoul, South Korea

continental squall line in east China fluctuate greatly depending on the evolution of the squall line. Fernandez-Raga et al. (2017) found that the RSD characteristics in Leon, Spain are associated with the directions of the cyclone path and of the moisture inflow. Using the RSD observations in Lausanne, Switzerland, Ghada et al. (2018) attributed the variability of the calculated RSD parameters for different weather types to the difference in the proportions of stratiform and convective rain. Loh et al. (2019) used RSD observations from Jincheon and Miryang in South Korea to analyze the RSD characteristics in the two regions according to three weather types.

The weather types that contribute most to precipitation depend on the region. Precipitation in South Korea is largely caused by the Changma front and typhoons in summer and by low-pressure systems in spring and autumn. The RSD characteristics of the three weather types have been studied for two rural regions in South Korea (Loh et al. 2019), but not for Seoul, the city with the largest population and most traffic in South Korea. Due to the environmental conditions in this city such as air pollution, the RSD characteristics of the weather types in Seoul can differ from those in the two rural regions.

This study examines the RSD characteristics in Seoul according to the weather type as well as the rain type using ground-based disdrometer data. Section 2 includes a description of the disdrometer and presents the data and methodology. The analysis results are presented and discussed in Section 3. Conclusions are given in Section 4.

2 Data and Methodology

2.1 Data

The disdrometer used in this study is the Parsivel² disdrometer manufactured by OTT Hydromet of Germany (Tokay et al. 2014) and is installed at Seoul National University (Fig. 1). The disdrometer measures the diameter and fall velocity of hydrometeor particles that fall through a sampling volume of 5.4 cm³ (18 cm long, 3 cm wide, and 0.1 cm high) with laser beams of 650-nm wavelength. The raw output consists of a 32 × 32 matrix whose entries are the number of particles corresponding to a size bin and a fall velocity bin. The sampling output interval is 1 min. The two smallest size bins are excluded from the analysis because of the low signal-to-noise ratio (Tokay et al. 2014) so that the particle size ranges from 0.25 to 26 mm. The fall velocity range is from 0 to 22.4 m s⁻¹. The disdrometer data are collected from May 2018 to July 2019.

A quality control process that removes observation errors is performed following Friedrich et al. (2013). First, the inaccuracies caused by strong winds are eliminated by excluding particles with diameters larger than 5 mm and fall velocities smaller than 1 m s⁻¹. Second, to eliminate inaccuracies caused by the particles falling at the edges of the sampling volume (Yuter et al. 2006),



Fig. 1 Photo of the disdrometer installed on the roof of the Atmospheric Environmental Observatory building, Seoul National University

particles with diameters smaller than 8 mm and fall velocities 60% greater than that following the fall velocity-diameter relationship according to Atlas et al. (1973), which correspond to the solid lines in Fig. 2a and Fig. 2b, are excluded (Jaffrain and Berne 2011). Finally, inaccuracies due to the splashing effect of the particles falling on the head surfaces of the instrument are eliminated by excluding particles smaller than 2 mm in diameter and with fall velocities smaller than 60% of that following the fall velocity-diameter relationship (Barthazy et al. 2004; Krajewski et al. 2006; Yuter et al. 2006). All data related to snow and hail particles are not considered in this study.

Following Thompson et al. (2015), the disdrometer data in 1-min interval with total drop counts of 100 or more during the three or more consecutive minutes of precipitation are analyzed and the data with $R < 0.05$ mm h⁻¹ are excluded. Additionally, both rain and drizzle are considered as rain. As a result, the data for the analysis of RSD characteristics consist of 33,583 1-min data.

2.2 Methodology

2.2.1 Description of Parameters

Using the disdrometer data, the raindrop concentration can be obtained from the following equation (Chen et al. 2017):

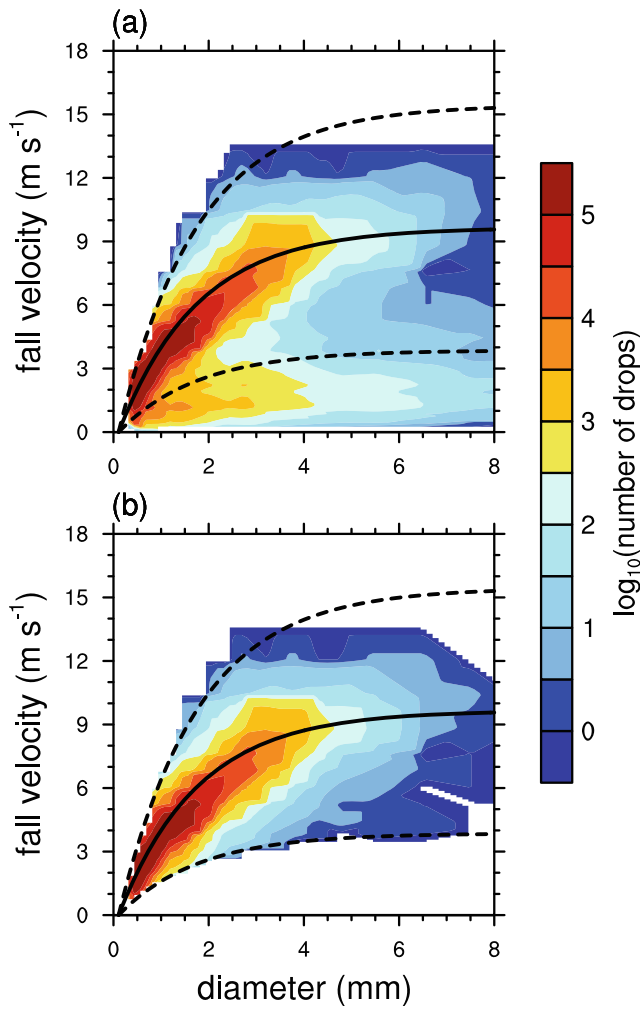


Fig. 2 Accumulated number of drops according to drop diameter and fall velocity for the observation period: (a) before and (b) after the quality control. The solid line indicates the fall velocity-diameter relationship of Atlas et al. (1973). The dashed lines indicate the $\pm 60\%$ of the fall velocity-diameter relationship

$$N(D_i) = \sum_{j=1}^{32} \frac{n_{ij}}{A_i V_j \Delta t \Delta D_i}, \tag{1}$$

where $N(D_i)$ ($\text{m}^{-3} \text{mm}^{-1}$) is the number concentration of raindrops per unit volume in the diameter range $D_i - \Delta D_i/2$ to $D_i + \Delta D_i/2$, n_{ij} is the number of raindrops belonging to size bin i and fall velocity bin j , A_i (m^2) is the effective sampling area of the size bin i (Tokay et al. 2014), V_j (m s^{-1}) is the fall velocity of the fall velocity bin j , and Δt (s) is the sampling time interval (60 s in this study). D_i and ΔD_i represent the mid-value and interval of the i -th size bin, respectively. Note that fall velocities measured by the disdrometer are used in this study, while some previous studies used terminal fall velocities as a function of drop diameter due to some uncertainty in the fall velocity measurements (Tokay et al. 2014; Janapati et al. 2020). Both methods are tested, and it is found that the

differences in the RSD parameters are small. The rainwater content W (g m^{-3}) and radar reflectivity Z ($\text{mm}^6 \text{m}^{-3}$) are expressed by the following equations:

$$W = \frac{10^{-3} \pi}{6} \rho_w \int D^3 N(D) dD \tag{2}$$

$$\approx \frac{10^{-3} \pi}{6} \rho_w \sum_{i=3}^{32} \sum_{j=1}^{32} D_i^3 \frac{n_{ij}}{A_i V_j \Delta t},$$

$$Z = \int D^6 N(D) dD \tag{3}$$

$$\approx \sum_{i=3}^{32} \sum_{j=1}^{32} D_i^6 \frac{n_{ij}}{A_i V_j \Delta t},$$

where ρ_w (g cm^{-3}) is the density of water.

The k th-order moment of the RSD is given by

$$M_k = \int D^k N(D) dD \tag{4}$$

$$\approx \sum_{i=3}^{32} D_i^k N(D_i) \Delta D_i.$$

The mass-weighted mean drop diameter D_m (mm) and the generalized intercept parameter N_w ($\text{m}^{-3} \text{mm}^{-1}$) are calculated using the following equations (Testud et al. 2001):

$$D_m = \frac{M_4}{M_3}, \tag{5}$$

$$N_w = \frac{4^4}{\pi \rho_w} \left(\frac{10^3 W}{D_m^4} \right). \tag{6}$$

The function most commonly used to express the RSD is the exponential distribution function, which is expressed as $N(D) = N_0 \exp(-\Lambda D)$ where N_0 is the intercept parameter ($\text{m}^{-3} \text{mm}^{-1}$) and Λ is the slope parameter (mm^{-1}). The parameter N_0 is generally assigned a fixed value, a representative example of which is $N_0 = 8 \times 10^3 \text{ m}^{-3} \text{mm}^{-1}$ from Marshall and Palmer (1948, MP48 hereafter). The exponential distribution parameters N_0 and Λ can be determined from M_2 and M_4 , which are expressed as follows (Zhang et al. 2008):

$$N_0 = \frac{M_2 \Lambda^3}{\Gamma(3)}, \tag{7}$$

$$\Lambda = \left[\frac{M_2 \Gamma(5)}{M_4 \Gamma(3)} \right]^{\frac{1}{2}}, \tag{8}$$

where Γ is the gamma function.

The generalized intercept parameter N_w is identical to the intercept parameter N_0 of an exponential size distribution that has the same W and D_m as in a gamma size distribution (Testud et al. 2001). In this study, N_w rather than N_0 is used

to facilitate classification of rain types (see subsection 2.2.2) and for direct comparison with previous studies that use N_w .

2.2.2 Rain-Type Classification

Rain is classified into stratiform, mixed, and convective rain types. The classification of the 33,583 1-min interval data follows the classification methods suggested by Bringi et al. (2009) and Thurai et al. (2016). Bringi et al. (2009) distinguished stratiform and convective rain based on the relationship between N_w and the median volume diameter D_0 calculated using observed RSDs. Thurai et al. (2016) introduced a likelihood index i that classifies rain into stratiform, mixed, and convective types as follows:

$$i = \log_{10}N_w - \log_{10}N_w^{sep}, \tag{9}$$

where N_w^{sep} is N_w on the line separating convective and stratiform data points on D_0 - $\log_{10}N_w$ plane given by

$$\log_{10}N_w^{sep} = -1.6D_0 + 6.3. \tag{10}$$

Stratiform, mixed, and convective rain are indicated by $i < -0.3$, $-0.3 \leq i \leq 0.3$, and $i > 0.3$, respectively. You et al. (2016) suggested modified D_0 - $\log_{10}N_w^{sep}$ relationships with different coefficients for a better classification of rain types in the southeastern region of the Korean Peninsula, but a commonly used relationship, Eq. (10), is used in this study.

2.2.3 Weather-Type Classification

Among various weather types that affect South Korea, the Changma front and low-pressure systems contribute most to rainfall (Rha et al. 2005), and they are used for the weather-type classification in this study. The Changma front (type CF) is a quasi-stationary front that causes heavy rainfall over the Korean Peninsula in summer. A low-pressure system (type L), responsible for a large portion of rainfall over the Korean Peninsula in spring and autumn, is a synoptic-scale system where a low-level migratory cyclone is coupled with an upper-level trough. Based on the weather maps, each day is

Table 1 The number of days of each weather type for each month. The numbers of days for May, June, and July are the sum of those from 2018 and 2019, while those for the other months are from either 2018 or 2019

Weather type	Month										total
	Mar	Apr	May	Jun	Jul	Aug	Sep	Oct	Nov	Dec	
CF	–	–	–	3	8	4	–	–	–	–	15
L	2	4	7	4	–	–	5	3	1	2	28

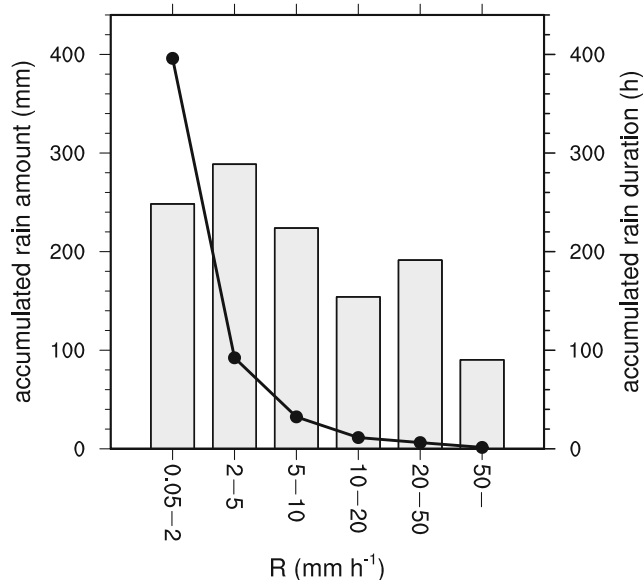


Fig. 3 Accumulated rain amount (grey bar) and accumulated rain duration (black solid line) for each rain rate category for the observation period

assigned the weather type that is judged to have dominantly affected the rainfall on that day. Rainy days with a daily accumulated rain amount smaller than 3 mm are excluded. The numbers of days determined to be type CF and type L are 15 and 28, respectively, and their monthly distributions are given in Table 1. Another weather type that contributes much to precipitation in South Korea is typhoons, but only a small number of typhoons produced rainfall in Seoul in the observation period and the rain amounts were small. For this reason, typhoons are not included in weather types.

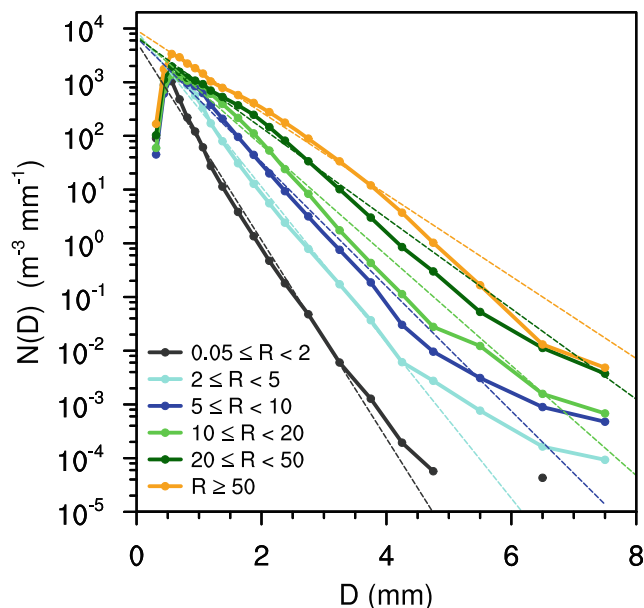


Fig. 4 Raindrop size distribution (solid lines) and corresponding exponential distribution (dashed lines) for each rain rate category for the observation period

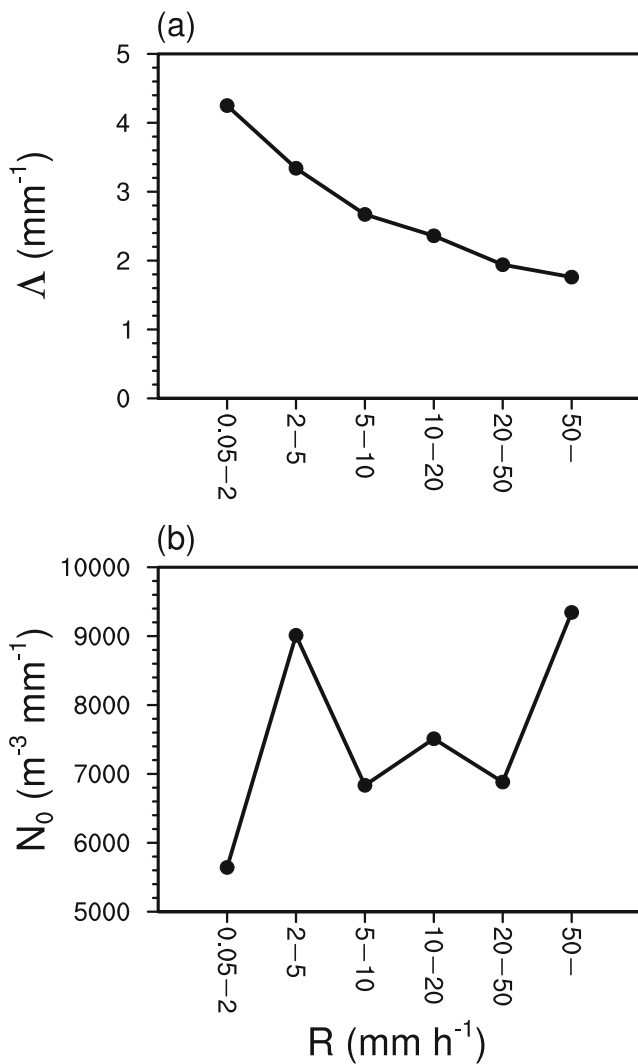


Fig. 5 (a) Slope parameter and (b) intercept parameter for each rain rate category

3 Results and Discussion

3.1 Characteristics of RSD According to Rain Rate

Previous studies have shown that RSDs have different characteristics depending on rain rate (Waldvogel 1974; Tokay

and Short 1996). In this study, the rain rate R is categorized into six categories. Figure 3 shows the accumulated rain amount and rain duration for six rain rate categories ($0.05 \text{ mm h}^{-1} \leq R < 2 \text{ mm h}^{-1}$, $2 \text{ mm h}^{-1} \leq R < 5 \text{ mm h}^{-1}$, $5 \text{ mm h}^{-1} \leq R < 10 \text{ mm h}^{-1}$, $10 \text{ mm h}^{-1} \leq R < 20 \text{ mm h}^{-1}$, $20 \text{ mm h}^{-1} \leq R < 50 \text{ mm h}^{-1}$, and $R \geq 50 \text{ mm h}^{-1}$) for the period from May 2018 to July 2019. The first three rain rate categories take up 64% of the total rain amount with a maximum at the second rain rate category ($2 \text{ mm h}^{-1} \leq R < 5 \text{ mm h}^{-1}$), and the last rain rate category ($R \geq 50 \text{ mm h}^{-1}$) contributes least to the total rain amount. The accumulated rain duration rapidly decreases with rain rate with the largest contribution to the total rain duration by the first rain rate category ($0.05 \text{ mm h}^{-1} \leq R < 2 \text{ mm h}^{-1}$) at 73% and a negligible contribution by the last two categories ($20 \text{ mm h}^{-1} \leq R < 50 \text{ mm h}^{-1}$ and $R \geq 50 \text{ mm h}^{-1}$). Note that despite the negligible contribution to the total rain duration, the accumulated rain amount for the last two categories is still significant.

The RSDs for the six different rain rate categories are obtained by averaging the 1-min interval disdrometer data for each category (Fig. 4). N_0 and Λ corresponding to the mean RSD for each category are calculated using Eqs. (7) and (8) and determine the exponential distribution. For all rain rate categories, the number concentration increases rapidly up to 0.562 mm in diameter and then decreases. For a given diameter of 0.812 mm or greater, the number concentration increases with increasing rain rate. These results are consistent with previous studies (Niu et al. 2010; Chen et al. 2017; Wu et al. 2019). Note that the discontinuity of the RSD for the first rain rate category in Fig. 4 (isolated black dot) is caused by the fact that no data exist for diameters over 5 mm except for the few with diameters between 6 and 7 mm. The exponential distributions are overall good representations of the RSDs although how well they are represented varies depending on the rain rate category.

The slope parameter decreases with rain rate from 4.25 mm^{-1} for the first rain rate category to 1.76 mm^{-1} for the last rain rate category (Fig. 5a). The slope parameter decreases more steeply when rain rate is small compared to when rain rate is large. The relationship between R and Λ in Fig. 5a is well represented by the power-law relationship $\Lambda = aR^b$

Table 2 Mean and standard deviation values (in parentheses) of the mass-weighted mean diameter, the logarithm of generalized intercept parameter, the slope parameter, and the radar reflectivity and the number of 1-min data for each rain rate category

Rain rate (mm h ⁻¹)	D_m (mm)	$\log_{10}[N_w \text{ (m}^{-3} \text{ mm}^{-1})]$	Λ (mm ⁻¹)	Z (dBZ)	# of data
0.05-2	0.86 (0.27)	3.87 (0.60)	4.56 (1.28)	17 (6.4)	23,764
2-5	1.18 (0.35)	4.05 (0.57)	3.34 (0.87)	29 (3.6)	5539
5-10	1.46 (0.37)	3.94 (0.47)	2.67 (0.58)	35 (2.9)	1946
10-20	1.61 (0.32)	4.01 (0.35)	2.38 (0.38)	39 (2.5)	683
20-50	1.96 (0.37)	3.95 (0.31)	1.97 (0.27)	45 (2.4)	377
50-	2.20 (0.25)	4.05 (0.23)	1.76 (0.17)	50 (1.6)	83

Table 3 As in Table 2, but for each rain type

Rain type	D_m (mm)	$\log_{10}[N_w \text{ (m}^{-3} \text{ mm}^{-1})]$	Λ (mm ⁻¹)	Z (dBZ)	# of data
stratiform	0.93 (0.32)	3.86 (0.59)	4.32 (1.32)	19 (8.4)	30,796
mixed	1.35 (0.45)	4.21 (0.61)	3.06 (1.12)	34 (5.9)	2339
convective	2.18 (0.54)	3.77 (0.58)	1.81 (0.30)	46 (3.1)	448

with $a = 4.03$ and $b = -0.20$. The intercept parameter fluctuates with rain rate (Fig. 5b). In particular, the N_0 values for the rain rate categories $2 \text{ mm h}^{-1} \leq R < 5 \text{ mm h}^{-1}$ and $R \geq 50 \text{ mm h}^{-1}$ are 13% and 17% larger than the constant N_0 from MP48, respectively. Unlike MP48, where only stratiform rain is considered, this study also considers mixed and convective rain. This might have contributed to the fact that the power-law relationship in this study has the a and b slightly smaller in magnitude than those in MP48 as well as the fluctuation in N_0 not seen in MP48.

The mass-weighted mean diameter, the logarithm of generalized intercept parameter, the slope parameter, and the radar reflectivity are calculated for each 1-min data, and their mean and standard deviation values are computed for each rain rate category (Table 2). Note that in Table 2 (also in Tables 3, 4 and Figs. 7d, 10d, 11d), the radar reflectivity Z is in dBZ. The mean values of D_m and Z monotonically increase with rain rate as can be expected from Fig. 4. The mean value of $\log_{10}N_w$, however, fluctuates with rain rate between 3.87 and 4.05. This result is different from that based in Busan on the southeast coast of the Korean Peninsula reported by You and Lee (2015) where the mean value of $\log_{10}N_w$ monotonically increases with rain rate. It is also noteworthy that the standard deviation values of $\log_{10}N_w$, Λ , and Z monotonically decrease with rain rate, implying that the RSD characteristics are more diverse for small rain rates.

3.2 Characteristics of RSDs According to Rain Types

The 1-min interval disdrometer data for the observation period are classified into the three rain types. Stratiform, mixed, and convective rain account for 50%, 28%, and 22% of the total rain amount, respectively, and the numbers of 1-min data for the three rain types are 30,796, 2339, and 448, respectively. The raindrop size distributions for the three rain types are presented in Fig. 6. The RSD for stratiform rain shows the steepest slope and the narrowest spectral width, while that for convective rain shows the mildest slope and the broadest

spectral width. The differences between the RSDs of different rain types can also be seen in the N_0 and Λ values of the corresponding exponential distributions obtained using the same method as in subsection 3.1. The slope parameter for stratiform rain is 3.58 mm^{-1} , which is larger than those for mixed (2.75 mm^{-1}) and convective (1.84 mm^{-1}) rain. The intercept parameters for stratiform, mixed, and convective rain are 4709, 9954, and $6193 \text{ m}^{-3} \text{ mm}^{-1}$, respectively.

Figure 7 shows the probability density functions (PDFs) for the mass-weighted mean diameter, the logarithm of generalized intercept parameter, the slope parameter, and the radar reflectivity for each rain type. The mean and standard deviation values of each parameter for each rain type are provided in Table 3. Figure 7a shows that the three different rain types have clearly distinguished PDFs for D_m . The unimodal distributions of convective and stratiform rain are clearly separated with the PDF for convective rain peaking at 2.03 mm and that for stratiform rain at 0.68 mm. Meanwhile, the distribution of mixed rain is more spread out than the other two rain types and its two peaks appear at 0.68 and 1.43 mm. The mean D_m value for convective rain is 2.18 mm, which is larger than that for stratiform (0.93 mm) or mixed (1.35 mm) rain. The PDF for $\log_{10}N_w$ of convective rain has the highest peak at 4.04 and a narrower distribution compared to that of stratiform rain which is more spread out and has the lowest peak appearing at 3.81 (Fig. 7b). Again, the $\log_{10}N_w$ distribution for mixed rain has two peaks, one of which appears at a large $\log_{10}N_w$ (4.94). The mean values of $\log_{10}N_w$ for stratiform, mixed, and convective rain are 3.86, 4.21, and 3.77, respectively.

The narrow distribution of Λ for convective rain has the highest peak at 1.95 mm^{-1} , whereas stratiform rain shows a more dispersed distribution over the larger Λ values compared to convective rain (Fig. 7c). The mean values of Λ for stratiform, mixed, and convective rain are 4.32, 3.06, and 1.81 mm^{-1} , respectively. Figure 7d shows clearly separated PDFs for Z amongst the three rain types with convective rain having the narrowest distribution with the largest mean Z value of 46 dBZ and stratiform rain having the broadest distribution with the smallest mean Z value of 19

Table 4 As in Table 2, but for each weather type

Weather type	D_m (mm)	$\log_{10}[N_w \text{ (m}^{-3} \text{ mm}^{-1})]$	Λ (mm ⁻¹)	Z (dBZ)	# of data
CF	1.03 (0.39)	3.85 (0.55)	3.98 (1.35)	22 (10.1)	6161
L	0.90 (0.32)	4.00 (0.56)	4.45 (1.35)	20 (8.9)	12,245

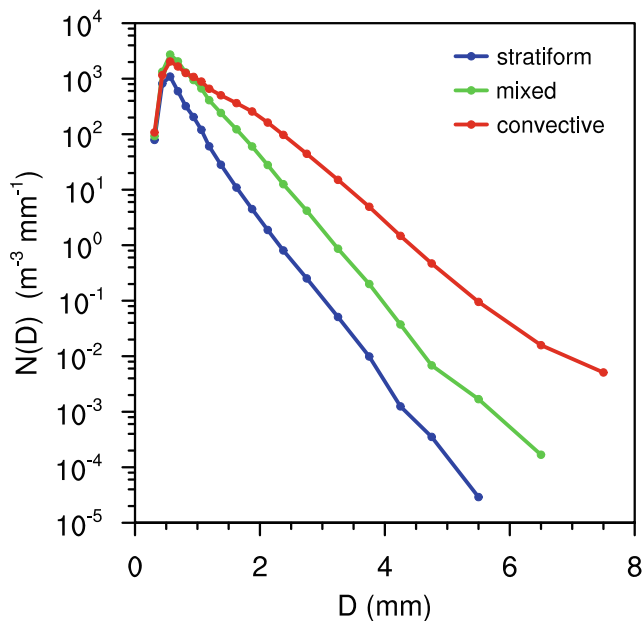


Fig. 6 Raindrop size distribution for each rain type

dBZ. The mean Z for mixed rain is 34 dBZ. The noticeably dispersed distributions of $\log_{10}N_w$, Λ , and Z for stratiform rain suggest the diversity within the stratiform rain in Seoul.

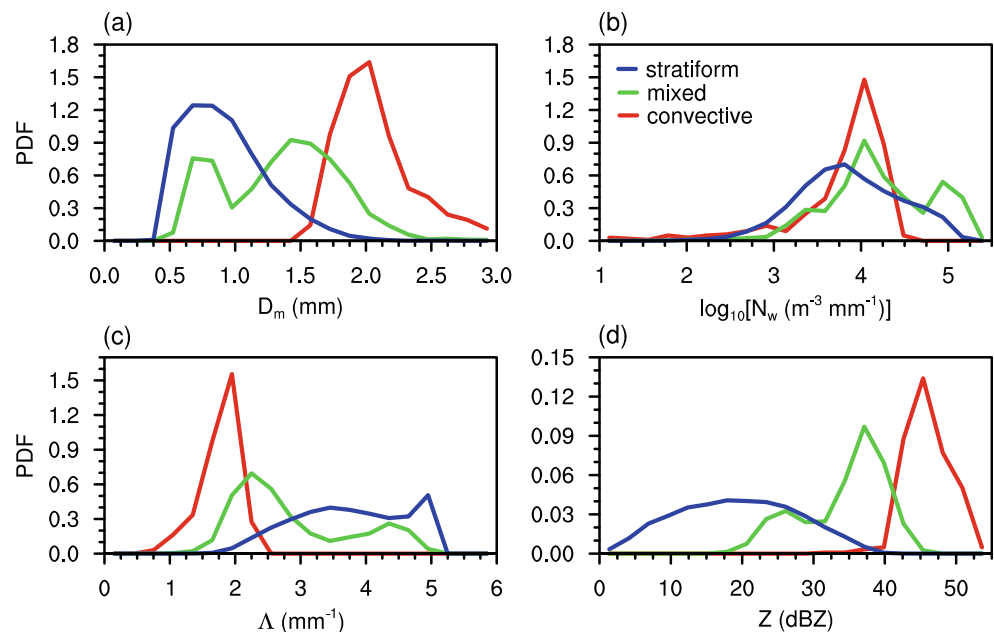
The mean D_m value of convective (stratiform) rain is larger (smaller) compared to that in Bringi et al. (2009). As for $\log_{10}N_w$, the mean values for both stratiform and convective rain in this study are larger compared to Bringi et al. (2009). These differences are thought to have originated from having different observation regions. The distributions of D_m for both stratiform and convective rain are clearly skewed and have positive skewness. For $\log_{10}N_w$, on the other hand, stratiform

rain has positive skewness, while convective rain has negative skewness. These results are different from Chen et al. (2013). Note that this study considers three rain types including mixed rain, whereas only two rain types are considered in Chen et al. (2013), which might be a contributing factor in these differences.

3.3 Characteristics of RSDs According to Weather Types

In this subsection, the RSD characteristics of the Changma front and low-pressure system are examined. Composite geopotential height, temperature, equivalent potential temperature, and wind vector fields are analyzed to see the large-scale thermodynamic and dynamic features associated with type CF and type L (Fig. 8). For this, the European Centre for Medium-Range Weather Forecasts (ECMWF) Reanalysis 5 (ERA5) hourly data with $0.25^\circ \times 0.25^\circ$ spatial resolution (Copernicus Climate Change Service, 2017) are used. For type CF, at 850-hPa level, the geopotential height contours extend in the southwest-northeast direction (Fig. 8c) and the wind blows parallel to the contours (Fig. 8e). The equivalent potential temperature field in Fig. 8e shows that warm and humid air enters the Korean Peninsula from the southwest. The large equivalent potential temperature gradient exists across the central region of the Korean Peninsula. At 500-hPa level, there is a warm air advection south of the Korean Peninsula and a weak trough is present northwest of the Korean Peninsula (Fig. 8a). For type L, at 850-hPa level, a well-developed trough is located immediately to the west of the Korean Peninsula (Fig. 8d). There are a cold advection west of the Korean Peninsula and a warm advection east of

Fig. 7 Probability density functions of (a) D_m , (b) $\log_{10}N_w$, (c) Λ , and (d) Z for each rain type



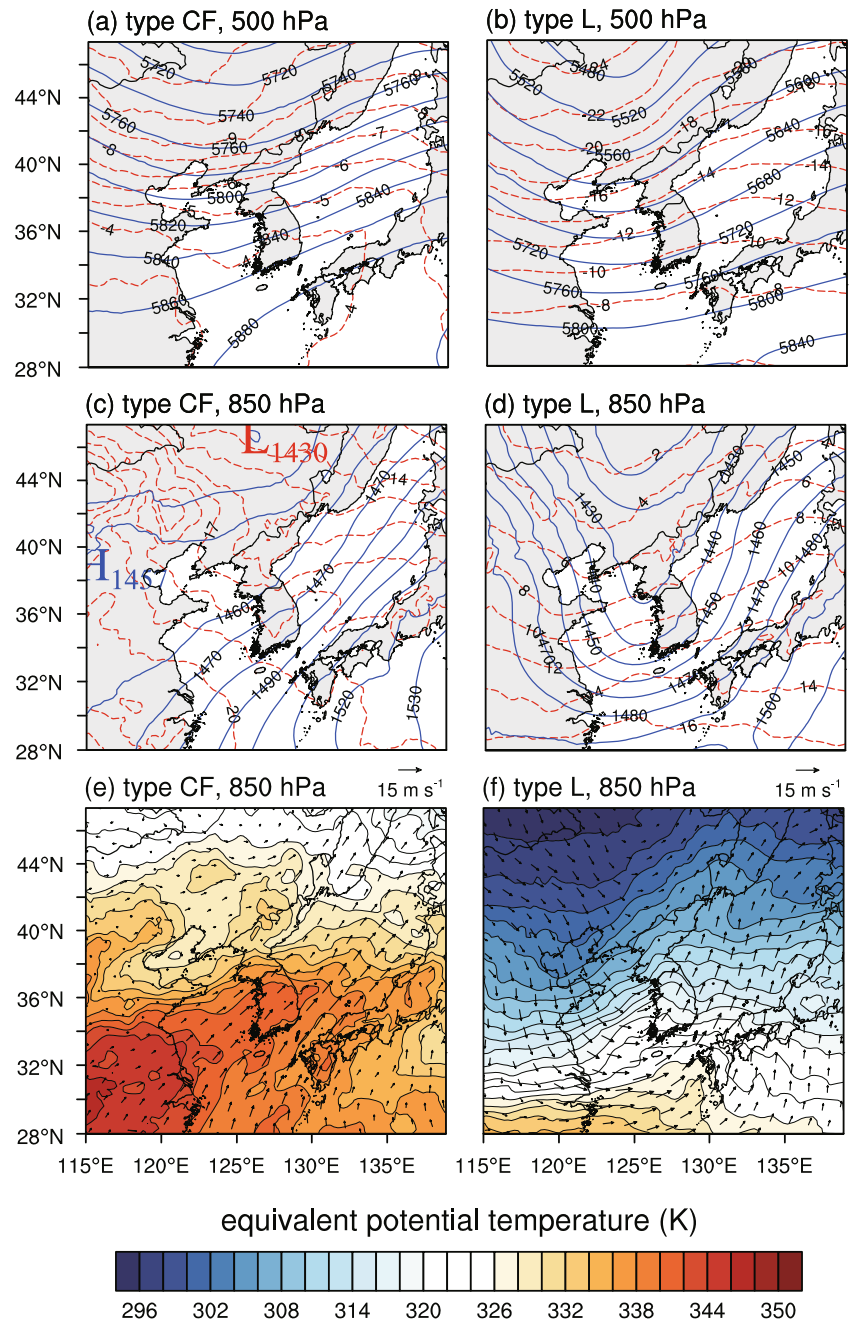
the Korean Peninsula (Fig. 8d, f). The trough at 500-hPa level is located to the west of the trough at 850-hPa level, which is an indication for the intensification of a surface low.

The raindrop size distributions for the Changma front and low-pressure system are presented in Fig. 9. The numbers of 1-min data used for type CF and type L are 6161 and 12,245, respectively. For raindrop diameters of 0.875 mm or greater, the number concentrations are larger for type CF than for type L. The RSD for type CF shows a milder slope compared to that for type L. Using the same method used in subsection 3.1, the intercept parameters and the slope parameters for the corresponding exponential distributions are computed. Type CF

has smaller N_0 and Λ ($3242 \text{ m}^{-3} \text{ mm}^{-1}$ and 2.68 mm^{-1}) compared to type L ($5459 \text{ m}^{-3} \text{ mm}^{-1}$ and 3.43 mm^{-1}).

The probability density functions for the mass-weighted mean diameter, the logarithm of generalized intercept parameter, the slope parameter, and the radar reflectivity for each weather type are presented in Fig. 10. The mean and standard deviation values of each parameter for each weather type are provided in Table 4. In Fig. 10a, both type CF and type L have positive skewness in the distribution of D_m , but type CF peaks at a larger D_m at 0.83 mm compared to type L (0.68 mm). The mean D_m values for type CF and type L are 1.03 and 0.90 mm, respectively. The PDFs for $\log_{10}N_w$ of type CF and type L

Fig. 8 Composite fields of geopotential height (blue solid lines) and temperature (red dashed lines) at (a) 500-hPa level and (c) 850-hPa level and (e) of equivalent potential temperature (shaded) and horizontal wind vectors at 850-hPa level for the Changma front. (b), (d), and (f) are the same as (a), (c), and (e), respectively, except for the low-pressure system



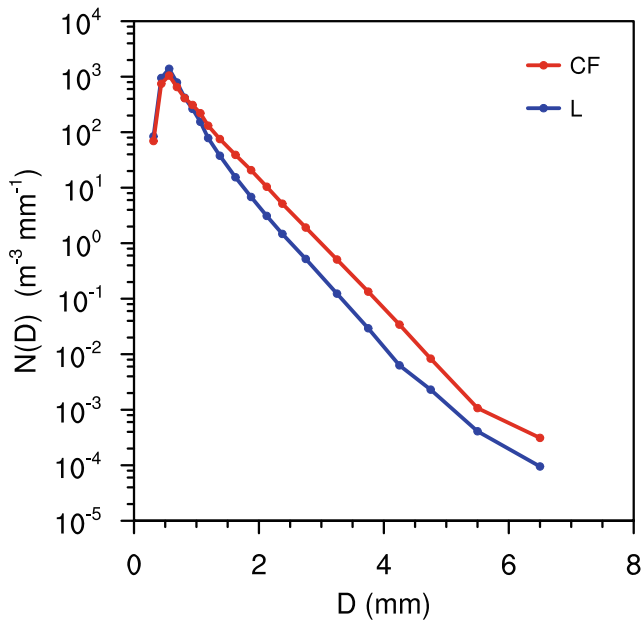


Fig. 9 Raindrop size distribution for each weather type (CF: Changma front and L: low-pressure system)

have peaks at 3.81 and at 4.04, respectively. The mean values of $\log_{10}N_w$ for type CF and type L are 3.85 and 4.00, respectively (Fig. 10b). In Fig. 10c, both type CF and type L exhibit two peaks in the PDFs for Λ similar to the bimodal shape of the PDF for Λ of stratiform rain (Fig. 7c). Note that the second peak corresponding to larger Λ values is higher for type L than for type CF. For Z values greater than 30 dBZ, the PDF of type CF is noticeably higher than that of type L. The mean values of Z for type CF and type L are 21 and 20 dBZ, respectively.

Note that the differences in the PDFs between type CF and type L are not as dramatic as those amongst different rain

types as seen in Fig. 7. This can be explained by the fact that the two weather types consist of all three rain types albeit in different proportions; type CF is comprised of 34% stratiform rain and 33% convective rain, whereas type L is comprised of 65% stratiform rain and 9% convective rain. Accordingly, it is noted that the PDFs of type CF shows raindrops with larger mean diameters, milder RSD slopes, and higher radar reflectivities, which are closer to the characteristics of convective rain. This result is somewhat consistent with the results of Suh et al. (2016) who examined the RSD characteristics in Busan where the proportion of convective precipitation for type CF was found to be greater than that for spring and autumn precipitation which consist largely of type L.

It is also noteworthy that the two weather types have different RSD characteristics of mixed rain. Figure 11 shows the PDFs of RSD parameters for each weather type as in Fig. 10, but further classified according to rain types. The PDFs for stratiform and convective rain of one weather type are similar to those for the other. The PDFs for mixed rain, however, show notable differences between the two weather types. The PDF of each RSD parameter for mixed rain was found to have two peaks (Fig. 7). One of these peaks is close to that for stratiform rain and the other is close to that for convective rain, for all parameters except $\log_{10}N_w$. The PDF of each RSD parameter for mixed rain of each weather type also has two peaks, but the peak close to that for convective rain is higher for type CF than type L while the other peak close to that for stratiform rain is higher for type L than type CF for all parameters except $\log_{10}N_w$ (Fig. 11a–d). In other words, the PDFs for mixed rain of type CF (type L) more closely resemble those for convective (stratiform) rain than type L (type CF) does. This suggests that not only the proportion of convective

Fig. 10 Probability density functions of D_m , $\log_{10}N_w$, Λ , and Z for each weather type (CF: Changma front and L: low-pressure system)

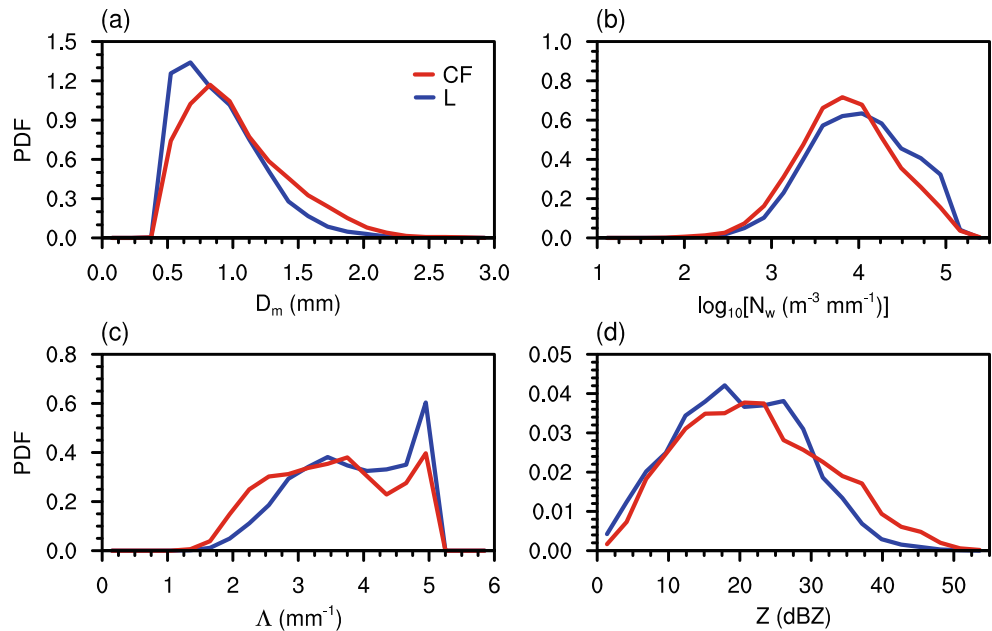
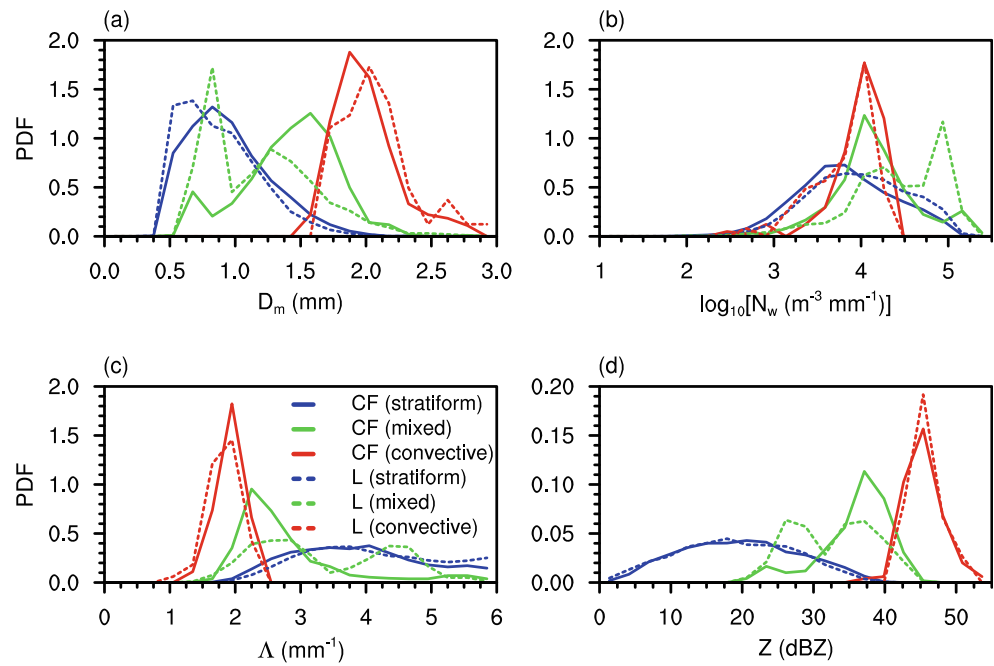


Fig. 11 Probability density functions of D_m , $\log_{10}N_w$, Λ , and Z for each weather type (CF: Changma front and L: low-pressure system), but further classified according to rain types



rain but also the mixed-rain characteristics of each weather type contribute to the RSD characteristics of the weather type. This also suggests that the double-peak structure of the PDFs of RSD parameters for mixed rain in Fig. 7 is largely affected by the two different RSD characteristics of mixed rain between type CF and type L.

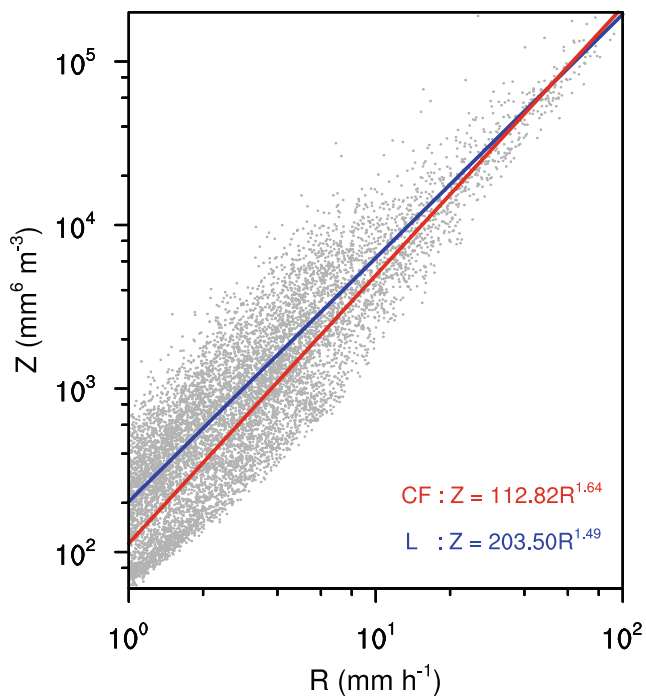


Fig. 12 Scatterplot of the Z – R pairs for each weather type. The fitted power-law relationships $Z = aR^b$ for the two weather types (CF: Changma front, L: low-pressure system) are indicated by red and blue solid lines, respectively

The quasi-stationary front that causes heavy rainfall during the East Asian summer monsoon is called the Changma front in Korea, the Baiu front in Japan, and the Meiyu front in China. The mean D_m value for the Changma front (1.03 mm) is smaller than what are reported for the Meiyu front (1.40 mm in Chen et al. 2013 and 1.27 mm in Wen et al. 2017) and the Baiu front (1.15 mm in Chen et al. 2019). The mean value of $\log_{10}N_w$ in this study (3.85) is larger than the mean value of $\log_{10}N_w$ for both the Meiyu front (3.55 in Chen et al. 2013 and 3.79 in Wen et al. 2017) and the Baiu front (3.59 in Chen et al. 2019). These differences suggest that the RSD characteristics vary from region to region even for the same weather type (weather phenomenon).

Figure 12 shows a scatterplot of radar reflectivity–rain rate pairs and the fitted power-law relationship for each weather type. The radar reflectivity generally increases with rain rate for both weather types. Compared to type L, type CF has a relatively small Z when R is smaller than $\sim 50 \text{ mm h}^{-1}$, while type CF has a relatively large Z when R is larger than $\sim 50 \text{ mm h}^{-1}$, which are indicated by the larger exponent of the power-law relationship for type CF. This stronger dependence of Z on R in type CF suggests that the number of large

Table 5 Mean values of lifting condensation level (LCL), convective available potential energy (CAPE), and cloud top height (CTH) for each weather type

Weather type	LCL (m AGL)	CAPE (J kg^{-1})	CTH (m AGL)
CF	540	604	9704
L	1250	84	7606

raindrops depends more highly on rain rate in type CF than in type L. For a given value of Z , $6000 \text{ mm}^6 \text{ m}^{-3}$ ($\sim 38 \text{ dBZ}$) for example, the rain rate for type CF (11.3 mm h^{-1}) is greater than that for type L (9.7 mm h^{-1}). The Z - R pairs may be better represented if the power-law relationship is separated for different weather types.

To identify possible causes for the differences in RSD characteristics between the two weather types, the mean values of lifting condensation level (LCL) and convective available potential energy (CAPE) for each weather type at the disdrometer location are calculated using ERA5 hourly data (Table 5). LCL and CAPE are averaged only over rainy periods with positive CAPE. Also, the mean cloud top height (CTH) is calculated using the Communication, Ocean and Meteorological Satellite (COMS) data with 15-min interval and horizontal grid spacing of 4 km provided by the National Meteorological Satellite Center, South Korea (Table 5). Since COMS does not provide cloud base height information, LCL is used to roughly estimate cloud base height. The higher CTH ($\sim 2 \text{ km}$ difference) and lower LCL for type CF indicate that type CF has a greater cloud thickness than type L. CAPE values are smaller than expected since they are averaged over the rainy periods during which moist convection can act to reduce thermodynamic instability, that is, CAPE. CAPE for type CF is 604 J kg^{-1} which is larger than that for type L (84 J kg^{-1}), indicating that clouds of type CF can be more convective.

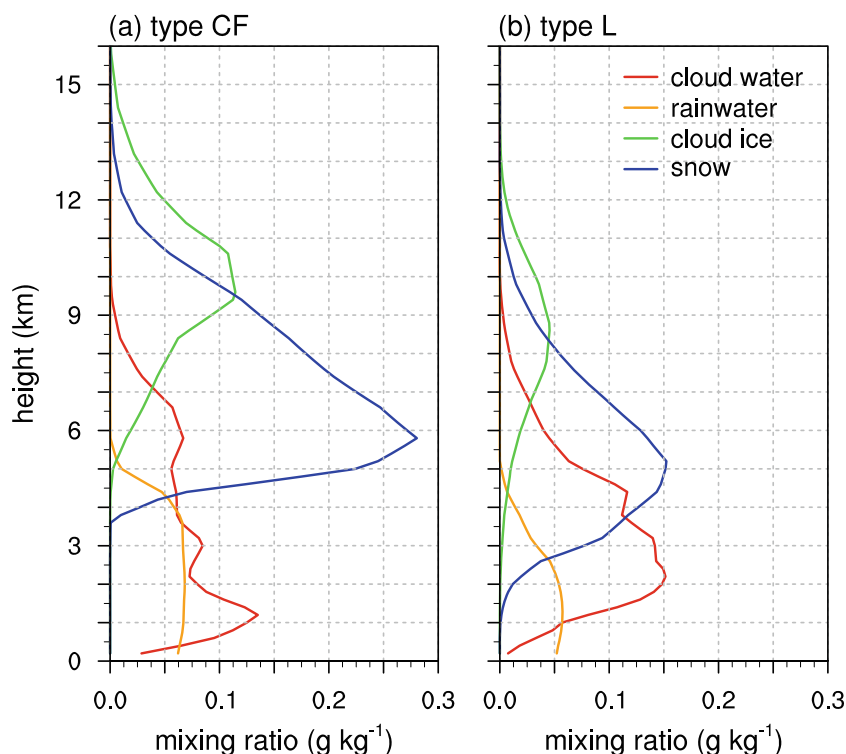
The composite vertical profiles of hydrometeor mixing ratios for each weather type at the disdrometer location are

computed by averaging ERA5 hourly data over the rainy periods (Fig. 13). Hydrometeors exist up to higher altitudes ($z \sim 16 \text{ km}$ for type CF and $z \sim 13 \text{ km}$ for type L) than the mean cloud top height obtained using COMS data largely because the averaging of cloud top heights is done over both high and low cloud top heights, which lowers the mean. The greater vertical development of clouds in type CF is partially attributed to the greater thermodynamic instability compared to type L. For type CF, cloud water accounts for a relatively small portion of clouds, suggesting that cloud water is efficiently converted into rain, cloud ice, and snow. The cloud water-to-rainwater conversion processes are essentially drop size increasing processes, and that these processes are more active in type CF may have contributed to the larger mean diameter of drops in type CF. A substantial portion of clouds in type CF are composed of cloud ice and snow, which implies active ice microphysical processes. Since large raindrops can be produced by melting of snow particles, the larger amount of snow in type CF may have also contributed to the greater number concentration of large raindrops in type CF compared to type L. These possible mechanisms need to be verified in detail using a sophisticated numerical model.

4 Conclusions

Using disdrometer data, this study examines the RSD characteristics in Seoul according to rain (stratiform, mixed, and convective) and weather (CF and L) types. The three rain

Fig. 13 Composite vertical profiles of cloud water, rainwater, cloud ice, and snow mixing ratios for type (a) CF and (b) L (CF: Changma front, L: low-pressure system)



types show clear separations among their RSD characteristics. On the other hand, relatively small differences are seen between the RSD characteristics of the two weather types. In particular, type CF appears to exhibit the characteristics closer to convective rain, which is in agreement with the assessment that type CF consists of a higher proportion of convective rain than type L does. Examining the reanalysis and satellite data provides some evidence of type CF having more favorable conditions for strong vertical development of clouds and active ice microphysical processes than type L. These results further highlight the importance of taking into account the rain type composition in order to fully understand the RSD characteristics of a given weather type (weather phenomenon).

This study classified the RSD characteristics in Seoul according to rain and weather types over a relatively short observation period. A future study can additionally consider seasonal RSD characteristics while also taking advantage of longer-term observation data. In addition, a better understanding of RSD characteristics can be achieved by further expanding and refining the weather type classification by including typhoons as an additional weather type for example, so that it better reflects the diversity of weather phenomena affecting the Korean Peninsula. As illustrated in this study, even the same weather type (weather phenomenon) can yield different RSD characteristics depending on the region; as such, it would be worthwhile to also incorporate data collected from multiple disdrometer locations. Lastly, it would be interesting to see if implementing observation-based parameters in a numerical model can lead to improvements in regional precipitation prediction.

Acknowledgements The authors are grateful to the anonymous reviewer for providing valuable comments. This work was supported by the Research Institute of Basic Sciences funded by the National Research Foundation of Korea (NRF-2019R1A6A1A10073437) and also supported by the Korea Meteorological Administration Research and Development Program under Grant KMI 2020-00710.

References

- Atlas, D., Srivastava, R.C., Sekhon, R.S.: Doppler radar characteristics of precipitation at vertical incidence. *Rev. Geophys.* **11**, 1–35 (1973)
- Barthazy, E., Göke, S., Schefold, R., Högl, D.: An optical array instrument for shape and fall velocity measurements of hydrometeors. *J. Atmos. Ocean. Technol.* **21**, 1400–1416 (2004)
- Bringi, V.N., Williams, C.R., Thurai, M., May, P.T.: Using dual-polarized radar and dual-frequency profiler for DSD characterization: a case study from Darwin, Australia. *J. Atmos. Ocean. Technol.* **26**, 2107–2122 (2009)
- Chen, B., Yang, J., Pu, J.: Statistical characteristics of raindrop size distribution in the Meiyu season observed in eastern China. *J. Meteorol. Soc. Jpn.* **91**, 215–227 (2013)
- Chen, B., Hu, Z., Liu, L., Zhang, G.: Raindrop size distribution measurements at 4,500 m on the Tibetan Plateau during TIPEX-III. *J. Geophys. Res. Atmos.* **122**, 11092–11106 (2017)
- Chen, Y., Duan, J., An, J., Liu, H.: Raindrop size distribution characteristics for tropical cyclones and Meiyu-Baiu fronts impacting Tokyo, Japan. *Atmosphere*. **10**, 391 (2019)
- Copernicus Climate Change Service (C3S): ERA5: Fifth generation of ECMWF atmospheric reanalysis of the global climate. Copernicus Climate Change Service Climate Data Store (CDS). <https://cds.climate.copernicus.eu/cdsapp#!/home> (accessed 10 December 2019) (2017)
- Das, S.K., Konwar, M., Chakravarty, K., Deshpande, S.M.: Raindrop size distribution of different cloud types over the Western Ghats using simultaneous measurements from Micro-Rain Radar and disdrometer. *Atmos. Res.* **186**, 72–82 (2017)
- Fernandez-Raga, M., Castro, A., Marcos, E., Palencia, C., Fraile, R.: Weather types and rainfall microstructure in Leon, Spain. *Int. J. Climatol.* **37**, 1834–1842 (2017)
- Friedrich, K., Karlina, E.A., Masters, F.J., Lopez, C.R.: Drop-size distributions in thunderstorms measured by optical disdrometers during VORTEX2. *Mon. Weather Rev.* **141**, 1182–1203 (2013)
- Ghada, W., Buras, A., Lüpke, M., Schunk, C., Menzel, A.: Rain microstructure parameters vary with large-scale weather conditions in Lausanne, Switzerland. *Remote Sens.* **10**, 811 (2018)
- Houze Jr., R.A.: *Cloud Dynamics*, 2nd edn. Academic Press, Oxford (2014)
- Jaffrain, J., Berne, A.: Experimental quantification of the sampling uncertainty associated with measurements from PARSIVEL disdrometers. *J. Hydrometeorol.* **12**, 352–370 (2011)
- Janapati, J., Seela, B.K., Lin, P.-L., Wang, P.K., Tseng, C.-H., Reddy, K.K., Hashiguchi, H., Feng, L., Das, S.K., Unnikrishnan, C.K.: Raindrop size distribution characteristics of Indian and Pacific Ocean tropical cyclones observed at India and Taiwan sites. *J. Meteorol. Soc. Jpn.* **98**, 299–317 (2020)
- Krajewski, W.F., Kruger, A., Caracciolo, C., Golé, P., Barthes, L., Creutin, J.-D., Delahaye, J.-Y., Nikolopoulos, E.I., Ogden, F., Vinson, J.-P.: DEVEX-disdrometer evaluation experiment: basic results and implications for hydrologic studies. *Adv. Water Resour.* **29**, 311–325 (2006)
- Loh, J.L., Lee, D.-I., You, C.-H.: Inter-comparison of DSDs between Jincheon and Miryang at South Korea. *Atmos. Res.* **227**, 52–65 (2019)
- Marshall, J.S., Palmer, W.M.: The distribution of raindrops with size. *J. Meteorol.* **5**, 165–166 (1948)
- Niu, S., Jia, X., Sang, J., Liu, X., Lu, C., Liu, Y.: Distributions of raindrop sizes and fall velocities in a semiarid plateau climate: convective versus stratiform rains. *J. Appl. Meteorol. Climatol.* **49**, 632–645 (2010)
- Pruppacher, H.R., Klett, J.D.: *Microphysics of Clouds and Precipitation*, 2nd edn. Springer, Dordrecht (2010)
- Rha, D.-K., Kwak, C.-H., Suh, M.-S., Hong, Y.: Analysis of the characteristics of precipitation over South Korea in terms of the associated synoptic patterns: a 30 years climatology (1973–2002). *J. Korean Earth Sci. Soc.* **26**, 732–743 (in Korean with English abstract) (2005)
- Seela, B.K., Janapati, J., Lin, P.-L., Wang, P.K., Lee, M.-T.: Raindrop size distribution characteristics of summer and winter season rainfall over north Taiwan. *J. Geophys. Res. Atmos.* **123**, 11602–11624 (2018)
- Sreekanth, T.S., Varikoden, H., Resmi, E.A., Kumar, G.M.: Classification and seasonal distribution of rain types based on surface and radar observations over a tropical coastal station. *Atmos. Res.* **218**, 90–98 (2019)
- Suh, S.-H., You, C.-H., Lee, D.-I.: Climatological characteristics of raindrop size distributions in Busan, Republic of Korea. *Hydrol. Earth Syst. Sci.* **20**, 193–207 (2016)
- Sui, C.-H., Tsay, C.-T., Li, X.: Convective-stratiform rainfall separation by cloud content. *J. Geophys. Res. Atmos.* **112**, D14213 (2007)

- Testud, J., Oury, S., Black, R.A., Amayenc, P., Dou, X.: The concept of “normalized” distribution to describe raindrop spectra: a tool for cloud physics and cloud remote sensing. *J. Appl. Meteorol.* **40**, 1118–1140 (2001)
- Thompson, E.J., Rutledge, S.A., Dolan, B., Thurai, M.: Drop size distributions and radar observations of convective and stratiform rain over the equatorial Indian and west Pacific oceans. *J. Atmos. Sci.* **72**, 4091–4125 (2015)
- Thurai, M., Gatlin, P.N., Bringi, V.N.: Separating stratiform and convective rain types based on the drop size distribution characteristics using 2D video disdrometer data. *Atmos. Res.* **169**, 416–423 (2016)
- Tokay, A., Short, D.A.: Evidence from tropical raindrop spectra of the origin of rain from stratiform versus convective clouds. *J. Appl. Meteorol.* **35**, 355–371 (1996)
- Tokay, A., Wolff, D.B., Petersen, W.A.: Evaluation of the new version of the laser-optical disdrometer, OTT Parsivel2. *J. Atmos. Ocean. Technol.* **31**, 1276–1288 (2014)
- Waldvogel, A.: The N_0 jump raindrop spectra. *J. Atmos. Sci.* **31**, 1067–1078 (1974)
- Wen, L., Zhao, K., Zhang, G., Liu, S., Chen, G.: Impacts of instrument limitations on estimated raindrop size distribution, radar parameters, and model microphysics during Mei-Yu season in East China. *J. Atmos. Ocean. Technol.* **34**, 1021–1037 (2017)
- Wen, L., Zhao, K., Wang, M., Zhang, G.: Seasonal variations of observed raindrop size distribution in East China. *Adv. Atmos. Sci.* **36**, 346–362 (2019)
- Wu, Z., Zhang, Y., Zhang, L., Lei, H., Xie, Y., Wen, L., Yang, J.: Characteristics of summer season raindrop size distribution in three typical regions of western Pacific. *J. Geophys. Res. Atmos.* **124**, 4054–4073 (2019)
- You, C.-H., Lee, D.-I., Jang, M., Kim, H.-K., Kim, J.-H., Kim, K.-E.: Variation of rainrate and radar reflectivity in Busan area and its measurement by cloud types. *Asia-Pacific J. Atmos. Sci.* **41**, 191–200 (2005)
- You, C.-H., Lee, D.-I.: Decadal variation in raindrop size distributions in Busan, Korea. *Adv. Meteorol.* **2015**(329327), (2015)
- You, C.-H., Lee, D.-I., Kang, M.-Y., Kim, H.-J.: Classification of rain types using drop size distributions and polarimetric radar: case study of a 2014 flooding event in Korea. *Atmos. Res.* **181**, 211–219 (2016)
- Yuter, S.E., Kingsmill, D.E., Nance, L.B., Löffler-Mang, M.: Observations of precipitation size and fall speed characteristics with in coexisting rain and wet snow. *J. Appl. Meteorol. Climatol.* **45**, 1450–1464 (2006)
- Zhang, G., Xue, M., Cao, Q., Dawson, D.: Diagnosing the intercept parameter for exponential raindrop size distribution based on video disdrometer observations: model development. *J. Appl. Meteorol. Climatol.* **47**, 2983–2992 (2008)
- Zhang, H., Zhang, Y., He, H., Xie, Y., Zeng, Q.: Comparison of raindrop size distributions in a midlatitude continental squall line during different stages as measured by Parsivel over East China. *J. Appl. Meteorol. Climatol.* **56**, 2097–2111 (2017)

Publisher's Note Springer Nature remains neutral with regard to jurisdictional claims in published maps and institutional affiliations.

